One-pot synthesis of novel ferric cubic mesoporous silica (Im3m symmetry) and its highly efficient adsorption performance

ARTICLE *in* JOURNAL OF MATERIALS CHEMISTRY · AUGUST 2011

Impact Factor: 7.44 · DOI: 10.1039/C1JM11877C

6 AUTHORS, INCLUDING:

Yu Zhou
Nanjing University of Technology
73 PUBLICATIONS **496** CITATIONS
SEE PROFILE

Ying Wang
Wright State University
267 PUBLICATIONS **2,657** CITATIONS
SEE PROFILE

Journal of Materials Chemistry

Cite this: J. Mater. Chem., 2011, 21, 13895

www.rsc.org/materials

PAPER

One-pot synthesis of novel ferric cubic mesoporous silica (*Im*3*m* symmetry) and its highly efficient adsorption performance†

Yu Zhou,[a] Jing Yang,[a] Jia Yuan Yang,[a] Fang Na Gu,[ab] Ying Wang*[bc] and Jian Hua Zhu*[a]

Received 29th April 2011, Accepted 30th June 2011
DOI: 10.1039/c1jm11877c

A novel facile route, denoted here as $I^0HO{\sim}COO^-S^+$, was reported to synthesize cubic *Im*3*m* mesoporous silicas and metal substituted analogues for the first time by utilizing commercial conventional cationic surfactant cetyltrimethylammonium bromide (CTAB) to direct the mesostructures along with citric acid as the acid media to give a weak acidic condition. This weak acidic system favors not only the fine phase control but also the optimal incorporation of ferric ions, providing a skilful way to prepare the mesoporous composites with a surprising adsorption capability. UV-vis DRS and ESR spectra indicated that the majority of the metal ions inserted into the siliceous framework within the tetrahedral coordination environment. Owing to the controllable incorporation of ferric species that form a monolayer on the channel wall plus the three-dimensional cage-like mesostructure that generates a fine geometric confinement towards the adsorbate, the mesoporous composite overruns zeolite NaY in the instantaneous adsorption of volatile nitrosamines and 1,3-butadiene for the first time.

Introduction

Endowing mesoporous silica with the high capability of adsorbing small volatile compounds to overrun zeolite is a great challenge, not only for the selective adsorption of molecular sieves, but also for materials science. Ordered mesoporous silica materials have the definitive advantage in the adsorption, separation and catalysis of bulky molecules due to their inherent large pore size and volume,[1–4] but often suffer from weak activity in capturing small molecules, distinctly inferior to zeolite. Unlike zeolite that has the numerous cations to attract adsorbate and the narrow channel to confine the tiny target, mesoporous silica materials lack both the fine geometric confinement and the electrostatic interaction toward the small adsorbate, owing to their essential wide channel structure with the amorphous pore walls. As a result, zeolite such as NaY always exhibits a superior adsorption capability over mesoporous silica materials in the instantaneous adsorption of volatile nitrosamines that is a strong class of carcinogens that widely exist in the environment.[5–7] Although many post-modifications have been tried to enhance the adsorptive capability of mesoporous silica,[8–11] it is hard to enable the modified MCM-41 to exhibit a comparable ability to NaY zeolite, let alone the mesoporous composites directly synthesized, because it is very difficult to create an efficient microenvironment inside their channel to capture a small volatile target like nitrosamines, which spurs us to seek a new synthesis strategy.

Among various mesoporous silicas, cubic mesoporous materials with three-dimensional (3D) interconnected pores and channels can provide more favorable mass-transfer kinetics than 2D mesoporous ones such as conventional MCM-41[1] or SBA-15.[2] For cubic mesoporous silica with the cages interconnected by small connecting windows, their special structure is able to generate extraordinary confinement toward guest compounds.[12,13] Thus anchoring metal ions on the cubic mesoporous silica with non-straight channels is selected as the synthesis strategy for the novel mesoporous adsorbent. Based on the method of "control of the hydrochloric acid to silicon molar ratio",[14] herein a novel synthetic route is used to construct a cubic *Im*3*m* symmetric mesostructure (cage type), in which citric acid is used to form weakly acidic conditions for fine phase transition control and feasible incorporation of ferric cations. In this low-cost synthetic route, strong hydrogen bonding of negative citrate anions will direct the assembly of the neutral silica species (I^0) through a new path named as $I^0HO{\sim}COO^-S^+$ by the cationic surfactant (S^+). To assess the performance of the resulting mesoporous composites in capturing small volatile molecules, two volatile nitrosamines, *N*-nitrosopyrrolidine

[a]*Key Laboratory of Mesoscopic Chemistry of MOE, College of Chemistry and Chemistry Engineering, Nanjing University, Nanjing, 210093, China. E-mail: jhzhu@netra.nju.edu.cn; Fax: (+86) 25-83317761; Tel: +025-83595848*
[b]*Department of Chemistry, College of Chemistry and Chemical Engineering, Nanjing University, Nanjing, 210093, China*
[c]*Ecomaterials and Renewable Energy Research Center (ERERC), Nanjing University, Nanjing, 210093, China*

† Electronic supplementary information (ESI) available: synthesis of FeMCM-41, FTIR spectra, wide angle XRD patterns, adsorption profiles fitted with Freundlich and Langmuir equation, the profile of NO_x released in the TPSR process of NNN. See DOI: 10.1039/c1jm11877c

(NPYR) and *N*-nitrosohexamethyleneimine (NHMI), along with 1,3-butadiene are chosen as the adsorbates; while instantaneous adsorption is utilized because the contact time between the adsorbate and adsorbent is less than 0.1 s in this strict test. We seek this new functional material, not only to compensate the inherent drawback of mesoporous silica in adsorption, but also to meet the rigorous requirements of environment protection.

Experimental section

N-Nitrosopyrrolidine (NPYR), *N*-nitrosohexamethyleneimine (NHMI) and *N*′-nitrosonornicotine (NNN) are purchased from Sigma, other reagents used here are A.R. grade and commercial available.

The pure siliceous silicas were prepared as follows: cetyltrimethylammonium bromide ($C_{16}H_{33}(CH_3)_3NBr$, CTAB) was dissolved in deionized water, and then the calculated amount of citric acid (HCA) and sodium citrate ($CANa_3$) were added to obtain a clear solution. After adding tetraethyl orthosilicate (TEOS) under vigorous stirring at 303 K, the mixture had the molar composition of TEOS/CTAB/HCA/$CANa_3$/H_2O = 1/0.2/1/*x*/500, and it was continuously stirred at room temperature for a further 48 h. Finally, the resulting solid was filtered, washed with deionized water and air-dried. Metal substituted analogues were synthesized in a similar way but adding a citrate salt such as ferric citrate (FeCA) to the initial reaction solution. The template free samples were prepared by calcination at 823 K for 5 h or by refluxing in ethanol.

X-Ray diffraction (XRD) patterns of samples were recorded on an ARL XTRA diffractometer in the 2θ range of 0.6–5° or 5–80°. Transmission electron microscopy (TEM) analysis was performed on a JEM-2100 (JEOL) electron microscope operating at 200 kV. Nitrogen adsorption isotherms were measured at 77 K on a Micromeritics ASAP 2020 volumetric adsorption analyzer, in which the sample was outgassed in the degas port of the apparatus at 573 K for 4 h prior to test. The BET specific surface area was calculated using adsorption data acquired at a relative pressure (P/P_0) range of 0.05–0.22 and the total pore volume was determined from the amount adsorbed at a relative pressure of about 0.99. The pore size distribution (PSD) curves were calculated from the analysis of the adsorption branch of the isotherm using the Barrett–Joyner–Halenda (BJH) algorithm. In the initial period of the synthesis, the pH value of the reaction mixture without TEOS was measured by using a pH meter, model PHS-3C. The Fe content of the samples was measured using a VARI AN AA240FS Fast sequential Atomic Absorption Spectrometer, while copper and magnesium contents were measured by ARL-9800 X-ray fluorescence analysis. Compressed KBr pellets containing 2-wt% of samples were used to get the FTIR spectra of synthesized mesoporous silica, and the spectra were recorded on a Bruker 22 infrared spectrophotometer with a resolution of 2 cm^{-1}. UV-vis DRS measurements were performed on a UV-2500 (Shimadzu) spectrophotometer adapted with a praying mantis accessory using $BaSO_4$ as a standard, and the adsorption spectra were obtained by converting the reflection data through the Kubelka–Munk formula. X-band ESR (9.7 GHz) spectra were recorded at 77 K using a BRUKER EMX-10/12 spectrometer. Solid state ^{29}Si MAS NMR measurement was performed with a 7.0 mm MAS probe on a Bruker Avance III spectrometer.

Temperature-programmed reduction (TPR) was carried out in a quartz U-tube reactor. 80 mg of sample was activated in a N_2 stream at 423 K for 1 h. After being cooled to room temperature, a H_2–Ar mixture (7% H_2 by volume, 40 mL min^{-1}) was switched on and the temperature was increased linearly at a rate of 10 K min^{-1}. The consumption of hydrogen in the stream was detected by a thermal conductivity detector.

Instantaneous adsorption of nitrosamines was carried out by the use of a gas chromatography (GC) method as previously reported.[15] 5 mg sample was directly heated to 453 K in the flow of carrier gas with a rate of 30 mL min^{-1} and then the solution of nitrosamine was pulse injected with the amount of 2 μL each time. The gaseous effluent was analyzed by an on-line Varian 3380 gas chromatograph to assess the adsorption of nitrosamines. Temperature program surface reaction (TPSR) experiments were performed as follows: 40 mg samples (20–40 mesh) were activated in N_2 flow at 773 K for 2 h and then cooled to 313 K, followed by the injection of 100 μL solution of NNN (5 mg mL^{-1}). After adsorption, the sample was purged on N_2 flow for 0.2 h, then heated to 773 K at a rate of 8 K min^{-1} while the gaseous cracking products were detected every 20 K by the spectrometric method as described in the ref. 16.

Results and discussion

Ordered cubic mesoporous silica could be obtained with the assistance of sodium citrate ($CANa_3$) in the citric acid (HCA) aqueous solution. In this weak acidic system (the pH values of the initial solution are shown in Table S1†), the concentration of sodium citrate was vital for the formation of the cubic mesostructure: there would be no precipitation once sodium citrate was absent. In the case of low sodium citrate concentration (x = 0.5, where x denotes the molar ration of $CANa_3$/HCA), the obtained mesoporous silica displayed a typical XRD pattern of two-dimensional hexagonal pores with the symmetry of *p6mm*, identical to that of the less ordered MCM-41.[1] As the sodium citrate concentration rose to x = 1, the strongest peak shifted to low angle, and a new diffraction peak appeared in the 2θ range of 2–3°, indicating the distortion from *p6mm* symmetry. Well ordered mesoporous silica with *Im*3*m* symmetry was able to be obtained in the case of x = 1.5, denoted as CA. Further increasing the amount of sodium citrate would lead to the mesophase changing to *p6mm* symmetry as the value of x reached 2.0 and becoming less ordered when x reached 2.5, which means that the highly ordered cubic *Im*3*m* mesostructure only can be prepared with the appropriate sodium citrate concentration of HCA/$CANa_3$/H_2O = 1/1.5/500. As shown in Fig. 1A, the low-angle XRD pattern of the resulting CA sample had the reciprocal spacing ($1/d_{hkl}$) ratios of $\sqrt{2}$: $\sqrt{4}$: $\sqrt{6}$: $\sqrt{10}$: $\sqrt{12}$: $\sqrt{16}$, which could be indexed to (110), (200), (211), (310), (222) and (400) Bragg reflections of the *Im*3*m* (Q^{229}) space group according to the principle of crystallography. Compared to other typical *Im*3*m* symmetric mesoporous silicas, the CA sample exhibited a broader 110 diffraction peak, similar to the small pore mesoporous silicas synthesized by using ionic surfactant such as ASM-4,[17] but different from the products synthesized by using non-ionic surfactants like SBA-16,[18] FDU-1[19] and HOM-1.[20]

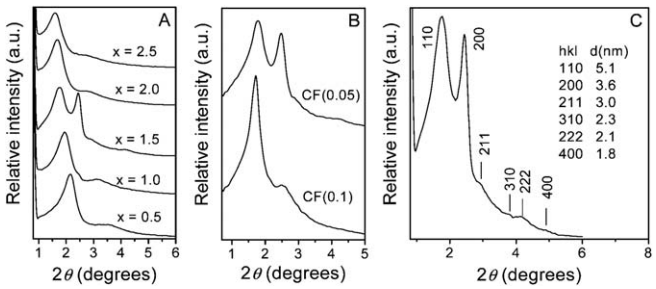

Fig. 1 Low-angle XRD pattern of (A) calcined samples synthesized with the molar ratio of TEOS/CTAB/HCA/$CANa_3$/H_2O 1.0/0.2/1.0/x/500, (B) ferric containing samples, and (C) magnified low angle XRD pattern of the CA sample.

And the relatively strong 200 diffraction peak may result from the slight orientation of the 3D structure in this synthetic system, which could also be observed on the *Im*3*m* symmetric film.[21] And the uniform mesoporous channel networks of the CA sample were observed in the TEM images to display the clear cubic lattice in the [100] or [110] direction (Fig. 2), indicative of a well oriented mesoporous system of cubic structure. The nitrogen sorption result of this sample demonstrated a type IV isotherm with a small H2-type hysteresis loop (Fig. 3), typical of small pores.[22–24] The CA sample had the BET surface area of 806 $m^2\ g^{-1}$ and the pore volume of 0.55 mL g^{-1}, and its most probable pore size was 3.3 nm (Table 1). There were 1716, 1588 and 1395 cm^{-1} bands in the FTIR spectrum of the as-synthesized CA sample (Fig. S1†), indexed as ν(C═O) in the –COOH group, ν_{as}(C═O) and ν_s(C═O) in the $–COO^-$ group[18] and indicating existence of citrate anions. These characteristic bands disappeared once the template was removed by refluxing in ethanol (the TG curve in

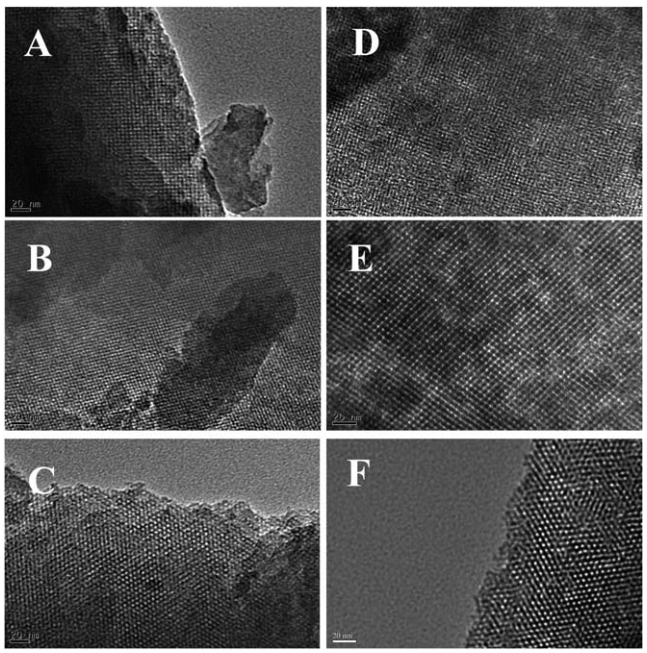

Fig. 2 TEM images of calcined CA sample recorded along the (A) [100], (B) [110], and (C) [111] directions and CF(0.1) along the (D) [100], (E) [110], and (F) [111] directions.

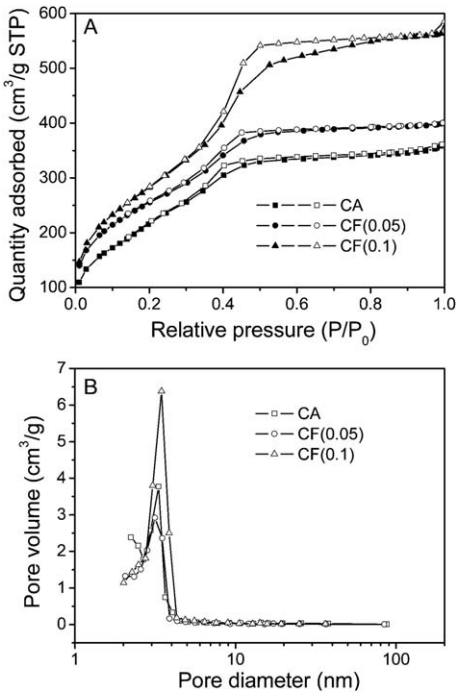

Fig. 3 (A) Nitrogen sorption isotherms and (B) pore size distribution of the CA and CF(y) series.

Fig. S2 indicates the remainder of only about 14% template in the refluxed CA sample) but they survived the sample being washed by water, due to the strong interaction between CTAB and citrate. The special weak acidic synthetic condition enables ferric mesoporous silica to be facilely fabricated. The ferric composite with *Im*3*m* symmetry, denoted as CF(y), was synthesized by adding ferric citrate in the initial reaction solution with the molar ratio of HCA/$CANa_3$/FeCA/H_2O = 1.0/1.5/y/500. Fig. 1B illustrates the low-angle XRD patterns of the CF(y) samples. Along with the enhancement of the ferric citrate concentration, the intensity of the (200) Bragg reflections declined but the reciprocal spacing ($1/d_{hkl}$) ratios remained the same. The space group of the CF(0.1) composite that was synthesized with the high ferric concentration could be still assigned to *Im*3*m* symmetry and was confirmed by the TEM image (Fig. 2), in which the well defined regular cubic pore lattice running over a larger area was observed. As shown in Fig. 3, all CF(y) samples had type IV isotherms in nitrogen sorption with the H2 type hysteresis loop that became larger and more obvious as their ferric content increased, and the H2 type hysteresis loop was known to be the characteristic of sharp capillary condensation in three-dimensional structures with small-cage-type mesopores.[22–24] Compared with the non-ferric parent, CF(y) composites had larger BET surface area and pore volume but the pore size remained constant, especially for CF(0.1) which had large values (1041 $m^2\ g^{-1}$ and 0.87 mL g^{-1}).

The Fe content of the composite was proportional to the amount of ferric citrate added to the initial synthetic system (Table 1), and the maximum value appeared for CF(0.1) because using more ferric citrate additives would lead to precipitation before adding the silica source. Absence of crystalline ferric oxide in the wide-angle X-ray diffraction of calcined the CF(y) samples

Table 1 The physical and adsorption properties of calcined composites synthesized in HCA/$CANa_3$/FeCA system

Sample	Molar ratio of metal/Si in gel[a]	Final metal (wt%)	d[b]/nm	S_{BET}[c]/m^2 g^{-1}	V_p[d]/mL g^{-1}	D_p[e]/nm	N_M/S_{BET}[f]/m^{-2}
CA	0	0	5.0	806	0.55	3.3	—
CF(0.05)	0.05	0.67	5.0	931	0.61	3.2	7.76×10^{16}
CF(0.1)	0.1	1.16	5.1	1041	0.87	3.4	1.20×10^{17}

[a] The initial molar composition is 1.0 TEOS/0.2 CTAB/1.0 HCA/1.5 $CANa_3$/y FeCA/500 H_2O. [b] d, the d-spacing value calculated from the Bragg's law. [c] S_{BET}, BET surface area. [d] V_p, total pore volume. [e] D_p, BJH mesopore diameter calculated from the desorption branch. [f] N_M/S_{BET}, the coverage surface of molecules per surface area calculated from $m_M M_M N_A/S_{BET}$, in which m_M, M_M and N_A are the weight of metal ion per one gram sample, molar weight of the metal ion and Avogadro constant respectively.

(Fig. S3†) proved the high dispersion of ferric species.[26] The UV-Vis DRS spectra of ferric species (Fig. 4) showed a strong broad adsorption in the range of 200–320 nm involving isolated framework Fe^{3+},[25] and this band could be unambiguously assigned to the ligand to metal charge-transfer (LMCT) that is consistent with tetrahedral sites of metal ions.[11,14,27–30] Particularly, it was attributed to the dπ–pπ charge transfer between the Fe and O atoms in the framework of Fe–O–Si,[31] similar to that reported in ferrisilicate materials containing tetrahedrally coordinated iron species.[32] Absence of the octahedral co-ordination ($Fe^{3+}O_6$) band below 320 nm in the spectrum of CF(0.05) (profile (a) in Fig. 4A) indicated that the sample was free of iron oligomer or ferric oxide.[11,27–30] This meant that the majority of ferric ions in the calcined composite existed in the tetrahedral coordination environment.[14,33] For the CF(0.1) sample with a relatively higher Fe content, a broad absorption tail appeared in the visible region (Fig. 4A) and meanwhile its color changed to pale orange, implying the existence of extra-framework ferric ions[25,32] that mainly located at the edge of the framework instead of forming bulky particles in the channel.[27] Nonetheless, the UV-vis DRS spectra of the as-synthesized samples (Fig. 4B) also showed the strong absorbency similar to that of the calcined analogues, where the band continued to 400 nm or higher region, originating from the low-energy charge transfer between the oxygen ligand and the central Fe^{3+} ion in tetrahedral symmetry.[11,14,25–32] It appears that ferric ions are coordinated to carbonyl groups in the as-synthesized samples whereas they are coordinated to –O–Si in the calcined products, and the change of ligands results in the extension of the absorbency band: the energy level of the dπ orbital in the O atoms of carbonyl is lower, and the dπ–pπ charge transfer between the Fe and O atoms in the as-synthesized sample is narrower than that in the calcined samples, yielding the shift of the LMCT bands.

On the other hand, two calcined CF(y) samples exhibited two obvious signals of $g = 4.3$ and $g = 2.0$ in their ESR spectra (Fig. 5), and the signal intensity rose as the Fe content was increased. According to literature and combining with the UV-vis DRS results, the signal at $g = 4.3$ is assigned to the strongly rhombic distorted tetrahedrally coordinated Fe^{3+} species originating from the middle Kramer's doublet respectively in the framework, while that at $g = 2.0$ can be attributed to the presence

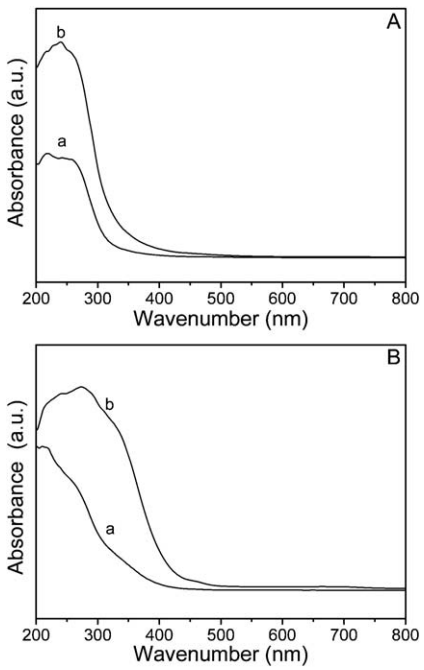

Fig. 4 UV-Vis DRS spectra of (A) calcined and (B) as-synthesized CF(y) series: (a) $y = 0.05$, (b) $y = 0.1$.

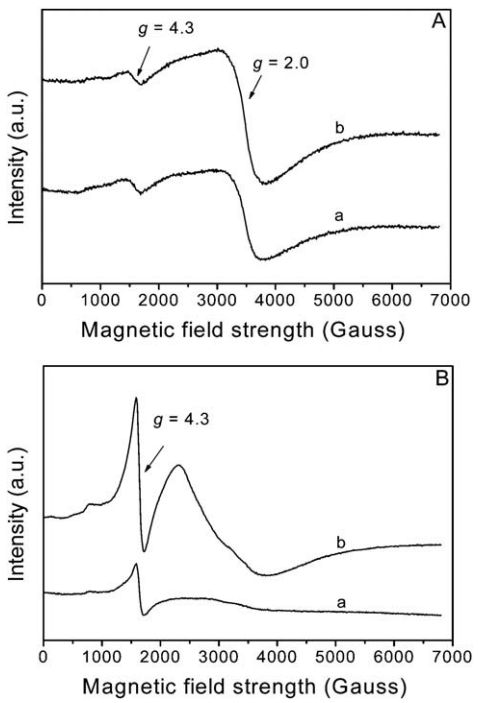

Fig. 5 ESR spectra of (A) calcined and (B) as-synthesized CF(y) series: (a) $y = 0.05$, (b) $y = 0.1$.

of high spin Fe^{3+} in a symmetrical tetrahedral coordination.[14,25,27,28,30] Together with the absence of the signal at $g = 2.2$, it is rationalized by proposing that most Fe cations locate in the tetrahedral coordination.[14] The TPR profile of the CF(0.1) sample (Fig. 6) showed only one peak centered at around 695 K that was associated with the reduction of 3-d Fe_2O_3 particles,[34] but a broad TPR peak continues to 973 K on Fe-MCM-41 that was prepared by direct synthesis and thus iron was present inside the silica framework.[35] These ferric species inside the framework were reduced at higher temperature due to the bonding of the silica matrix.[34,36] This difference indicates the good dispersion of ferric species on the channel walls of CF(0.1).

Fig. 7 displays the ^{29} Si NMR spectrum of CA and CF(0.1) samples and their fitting with multiple peaks. As shown in Fig. 8, the CA and CF(0.1) samples all exhibited three signals at around −105, −99 and −90 ppm that are assigned to Q^4 [$Si(OSi)_4$], Q^3 [$Si(OSi)_3(OH)$] and Q^2 [$Si(OSi)2(OH)2$] substructures, respectively. And one additional peak at −83 ppm can be observed for CF (0.1), which is attributed to the Q^{Fe} [$Si(OSi)_3Fe$] substructure. Fitting the spectrum with multiple peaks reveals that two samples have a similar silica condensation; for instance, they have almost the same ratio of $Q^4/Q^3/Q^2$. Owing to the formation of [$Si(OSi)_3Fe$] that costs the surface silanol group (Q^3 [$Si(OSi)_3(OH)$]), 1% percent of Q^3 [$Si(OSi)_3(OH)$] in the CF(0.1) sample changes to Q^{Fe} [$Si(OSi)_3Fe$] (Fig. 7B). In addition, such transition percentage is coincident with the ferric content of CF(0.1), further validating the monolayer dispersion of ferric ions.

Instantaneous adsorption of volatile nitrosamines at 453 K is the strict probe test due to the very short contact time of less than 0.1 s.[15] The siliceous CA sample weakly adsorbed NPYR and its capacity was soon saturated (Fig. 8A). Incorporating ferric ions dramatically facilitated the adsorption of volatile nitrosamines, and the CF(0.1) composite exhibited a surprisingly high capability: it captured the same amount of the carcinogen as that by zeolite NaY when the total amount of NPYR passed was lower than 0.7 mmol g^{-1}, which is unusual because NaY is the best zeolite adsorbent of NPYR to date.[8,15] Moreover, the CF(0.1) sample adsorbed more NPYR than zeolite NaY as the accumulated amount of NPYR increased: in the case where 2.0 mmol g^{-1} of NPYR was passed through the adsorbent, CF (0.1) trapped 1.76 mmol g^{-1} while NaY adsorbed 1.43 mmol g^{-1}.

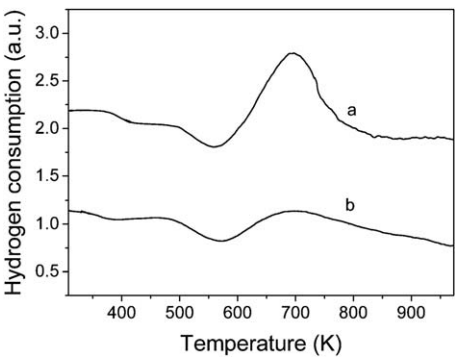

Fig. 6 Temperature-programmed reduction (TPR) profiles of)a) CF (0.1) and (b) FeMCM-41 (the synthesis is shown in the ESI†). These two samples had the same ferric content.

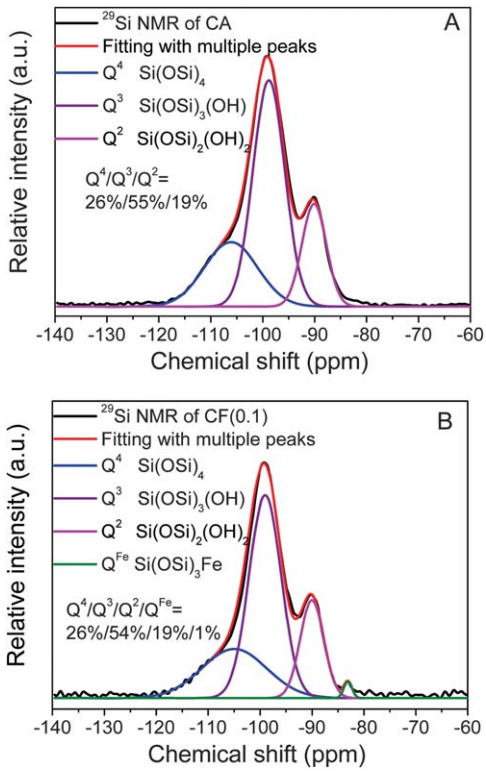

Fig. 7 ^{29}Si NMR spectra of (A) CA and (B) CF(0.1) samples and their fitting with multiple peaks.

This is the first time that a mesoporous composite has exceeded a zeolite in the instantaneous adsorption of volatile nitrosamines. As the total amount of NPYR reached 3.4 mmol g^{-1}, the superiority of CF(0.1) became much more obvious because it captured 79% (2.7 mmol g^{-1}) but zeolite NaY adsorbed only 53% (1.8 mmol g^{-1}). To deeply assess the adsorption capacity of the two samples, their experimental isotherms (Fig. 8A) are analyzed by fitting with the Freundlich equation ($\ln q = \ln K_F + (1/n)\ln C$) and the Langmuir equation ($1/q = 1/K_L/q_m/C + 1/q_m$), in which q and C are the amount of nitrosamine captured and that passed by per gram of adsorbent respectively, as shown in Fig. S5.† The exponent of $1 < n < 10$ in the Freundlich equation is associated with the favorable nature of the adsorption system so the smaller value favors a higher adsorptive strength and better favorability. CF(0.1) has a small n value of 1.1 throughout the whole isotherm while zeolite NaY displays a large n of 2.0 in the thick concentration of NPYR, and it is clear that CF(0.1) has a stronger adsorbate/adsorbent interaction than zeolite NaY. Referring to the Langmuir fitting isotherms (Fig. S5†), CF(0.1) demonstrates a large q_m of 11.0 mmol g^{-1}, the saturated adsorption amount, which was double that of zeolite NaY (3.1 mmol g^{-1}), thanks to the larger pore volume of the ferric mesoporous composite. Moreover, such a surprisingly superior adsorption also appeared on various mesoporous ferric composites synthesized with different molar ratios of raw materials, regardless of whether it had *Im3m* or *p6mm* symmetry. However, a cubic mesostructure and curved mesochannels will further enhance the adsorption performance. The CF(0.1) sample with *Im3m* symmetry and cage-type mesopores showed a higher performance than other

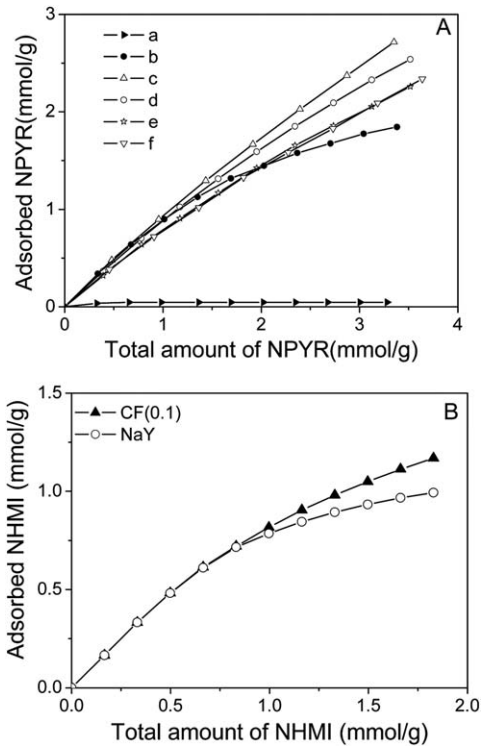

Fig. 8 Instantaneous adsorption of (A) NPYR and (B) NHMI on ferric containing mesoporous silica and NaY: (a) CA, (b) NaY, (c) CF(0.1), (d, e, f) are the ferric containing mesoporous silica materials synthesized with the molar ratio of 0.2 CTAB/1 HCA/x $CANa_3$/500 H_2O/y FeCA, in which x and y denote the molar ratio of $CANa_3$ and FeCA to CA respectively: (d) $x = 0.5$, $y = 0.05$; (e) $x = 1.0$, $y = 0.075$; (f) $x = 1.0$, $y = 0.15$. The textural properties of them are shown in Table S2 and Fig. S4.†

ferric containing samples with *p6mm* symmetry and straight mesochannels, although they contained a similar or higher concentration of ferric ions. In the instantaneous adsorption of NHMI (Fig. 8B), the another volatile nitrosamine with a seven-membered ring, CF(0.1) exhibited the same capacity as zeolite NaY when the total amount of NHMI was below 0.83 mmol g^{-1}, but exceeded the zeolite as the adsorption continued. The ferric composite captured 18% more NHMI (1.18 mmol g^{-1}) than NaY (1.0 mmol g^{-1}) as the total amount of NHMI reached 1.8 mmol g^{-1} (Fig. 8B), confirming the superiority of CF(0.1) in the adsorption of volatile nitrosamines. Moreover, CF(0.1) could capture the same amount of 1,3-butedinene as zeolite NaY in the instantaneous adsorption (Fig. 9), and its capability exceeded 0.45 mmol g^{-1}, which is also unprecedented because the SBA-15 modified with alumina only had the capacity of less than 0.25 mmol g^{-1} under the same conditions.[37] For the catalytic degradation of bulky tobacco specific nitrosamines such as *N′*-nitrosonornicotine (NNN), the CF(0.1) composite exhibited an inherently higher activity than zeolite NaY in the temperature programmed surface reaction test (Fig. S6†). It decomposed 28.1 μmol g^{-1} of NNN, four times more than NaY zeolite (4.84 μmol g^{-1} [38]). The maxima of NO_x desorption also shift towards lower temperature from 533 K (sample CA) to 492 K (sample CF(0.1), Fig. S6†), much lower than that of other mesoporous materials (570–590 K[5,38]), mirroring the strong promotion of ferric guest on the degradation of nitrosamines.

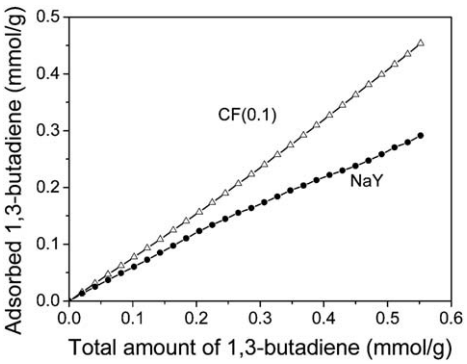

Fig. 9 Instantaneous adsorption of 1,3-butadiene on the CF(0.1) sample and NaY zeolite at room temperature.

The optimal distribution of ferric species in the CF(0.1) composite results in the success of exceeding zeolite in the adsorption of volatile compounds as demonstrated in Fig. 8A. However, such a controllable dispersion results from the special synthesis strategy. In the possible interaction scheme (Scheme 1), denoted as $I^0HO{\sim}COO^-S^+$ and tentatively drawn according to the electric charge matching principle, citrate anions stabilize the surfactant/silicate aggregates in two sides: they combine with the positive surfactant through the electrostatic interaction between carboxyl and surfactant (COO^-S^+), while also connecting with neutral silica species through hydrogen bonding (I^0HO). Such an enhanced interaction between surfactant and silica precursor causes the condensation of the silica species and thus the formation of mesoporous silica. However, these citrate anions in a gel still have unoccupied coordinate sites forward cations since citrate anion has four coordination atoms derived from one alcoholic hydroxyl and three carboxylic hydroxyls (Scheme 1) and they cannot totally interact with CTAB and silica precursors due to steric hindrance. Consequently, the ferric ion in solution incorporates with those citrate anions in the gel to form a special layer in the interface between the micelles and the assembled silica precursors. Unlike those ferric species deposited on the external surface of the assembled solid that will be removed unavoidably during the filtering and washing steps, these incorporated citrate anions are water-resistant and are preserved in the interface. However, they can be easily removed along with CTAB by refluxing with ethanol, and this difference indicated their location in the micelle. Once the sample is calcined to remove micelles, these ferric species will form the monolayer on

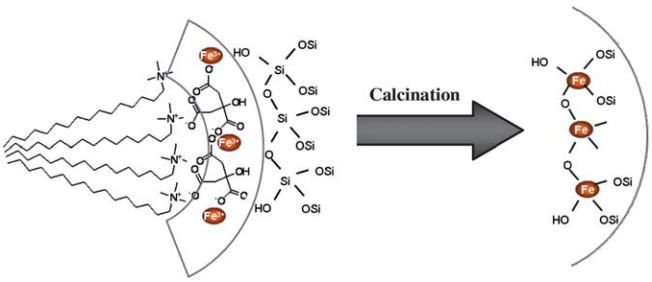

Scheme 1 Schematic illustration of site-specific coating of ferric ions into the siliceous framework during calcination.

the channel wall with the optimal accessibility (Scheme 1). It is these highly dispersed ferric species that attract the volatile compounds like NPYR in the instantaneous adsorption, through electrostatic interaction towards the N–NO group of NPYR with negative charge,[5,8,39] enabling the mesoporous composite to exceed zeolite for the first time. As is evident from Fig. 8A, the sample with either *Im*3*m* or *p*6*mm* symmetry was superior to zeolite NaY in the adsorption of NPYR at high concentration once it had the ferric species uniquely dispersed. This means that the mesoporous composite can be superior to zeolites in trapping small pollutant molecules, as long as the ferric modifier is able to be controllably incorporated on the channel walls of the host. Nonetheless, actually it is very hard, if not impossible, for the common post-modification to establish such an even dispersion of modifier on the mesoporous host because of the uncontrollable aggregation of the guest. One-pot synthesis also fails to locate the modifiers homogenously on the surface of channel walls, since some of the guests usually incorporate into the framework to become inaccessible. Only through this novel and facile route of $I^0HO{\sim}COO^-S^+$ can we realize the tunable dispersion of ferric species on mesoporous silica to create efficient adsorptive sites on the amorphous silica walls, and this strategy is proven to be versatile for various mesoporous materials in enhancing their adsorptive performance (Fig. 8A).

Conclusions

In summary, a new strategy is established to fabricate cubic mesoporous silica materials with *Im*3*m* symmetry by utilizing citric acid to form weakly acidic conditions. In this route, the electrostatic interaction and hydrogen bonding in the $I^0HO{\sim}COO^-S^+$ path provide the necessary driving force for the assembly of neutral silica species around the cationic surfactant (CTAB), producing 3D cubic *Im*3*m* symmetries. Moreover, ferric ions can be highly dispersed *in situ* on the silica framework, and the resulting functional material shows an excellent performance, for the first time, superior to that of zeolite NaY in the instantaneous adsorption of volatile nitrosamines. Thanks to the enhanced geometric confinement of the 3D channels and cage-type pores plus the strong electrostatic interaction of ferric species toward nitrosamines, this success represents a milestone for mesoporous materials to generate strong active sites comparable to zeolites and take effect of the large pore volume.

Acknowledgements

Financial support from NSF of China (20773601, 20873059 and 20871067), Grant 2008AA06Z327 of 863 Program of MSTC and National Basic Research Program of China (2007CB613301), the Scientific Research Foundation of Graduate School, and Analysis Center of Nanjing University is gratefully acknowledged.

Notes and references

1 J. S. Beck, J. C. Vartuli, W. J. Roth, M. E. Leonowicz, C. T. Kresge, K. D. Schmitt, C. T. W. Chu, D. H. Olson, E. W. Sheppard, S. B. McCullen, J. B. Higgins and J. L. Schlenker, *J. Am. Chem. Soc.*, 1992, **114**, 10834.
2 D. Y. Zhao, J. L. Feng, Q. S. Huo, N. Melosh, G. H. Fredrickson, B. F. Chmelka and G. D. Stucky, *Science*, 1998, **279**, 548.
3 Z. L. Yang, Y. F. Lu and Z. Z. Yang, *Chem. Commun.*, 2009, 2270.
4 I. I. Slowing, J. L. Vivero-Escoto, B. G. Trewyn and V. S.-Y. Lin, *J. Mater. Chem.*, 2010, **20**, 7924.
5 Y. Cao, L. Y. Shi, C. F. Zhou, Z. Y. Yun, Y. Wang and J. H. Zhu, *Environ. Sci. Technol.*, 2005, **39**, 7254.
6 B. Prokoczyk, D. Hoffmann, M. Bologna, A. J. Cunningham, N. Trushin, S. Akerkar, T. Boyiri, S. Amin, D. Desai, S. Colosimo, B. Pottman, G. Leder, M. Ramadani, D. Henne-Bruns, H. G. Beger and K. EI- Bayoumy, *Chem. Res. Toxicol.*, 2002, **15**, 677.
7 M. Izquierdo-Pulido, J. F. Barbour and R. A. Scanlan, *Food Chem. Toxicol.*, 1996, **34**, 297.
8 F. N. Gu, Y. Zhou, F. Wei, Y. Wang and J. H. Zhu, *Microporous Mesoporous Mater.*, 2009, **126**, 143.
9 F. N. Gu, F. Wei, J. Y. Yang, Y. Wang and J. H. Zhu, *J. Phys. Chem. C*, 2010, **114**, 8431.
10 P. Srinivasu and A. Vinu, *Chem.–Eur. J.*, 2008, **14**, 3553.
11 Y. M. Liu, J. Xu, L. He, Y. Cao, H. Y. He, D. Y. Zhao, J. H. Zhuang and K. N. Fan, *J. Phys. Chem. C*, 2008, **112**, 16575.
12 A. E. Garcia-Bennett, K. Lund and O. Terasaki, *Angew. Chem., Int. Ed.*, 2006, **45**, 2434.
13 A. E. Garcia-Bennett, K. Miyasaka, O. Terasaki and S. N. Che, *Chem. Mater.*, 2004, **16**, 3597.
14 A. Vinu, T. Krithiga, V. Murugesan and M. Hartmann, *Adv. Mater.*, 2004, **16**, 1817.
15 C. F. Zhou, Y. Cao, T. T. Zhuang, W. Huang and J. H. Zhu, *J. Phys. Chem. C*, 2007, **111**, 4347.
16 Y. Xu, J. H. Zhu, L. L. Ma, A. Ji, Y. L. Wei and X. Y. Shang, *Microporous Mesoporous Mater.*, 2003, **60**, 125.
17 A. E. Garcia-Bennett and O. Terasaki, *Chem. Mater.*, 2004, **16**, 813–821.
18 D. Y. Zhao, Q. S. Huo, J. L. Feng, B. F. Chmelka and G. D. Stucky, *J. Am. Chem. Soc.*, 1998, **120**, 6024.
19 C. Z. Yu, Y. H. Yu and D. Y. Zhao, *Chem. Commun.*, 2000, 575–576.
20 S. A. El-Safty and T. Hanaoka, *Chem. Mater.*, 2004, **16**, 384.
21 D. Y. Zhao, P. D. Yang, N. Melosh, J. L. Feng, B. F. Chmelka and G. D. Stuck, *Adv. Mater.*, 1998, **10**, 1380.
22 C. B. Gao, Y. Sakamoto, O. Terasaki, K. Sakamotoc and S. N. Che, *J. Mater. Chem.*, 2007, **17**, 3591.
23 C. B. Gao, H. B. Qiu, W. Zeng, Y. Sakamoto, O. Terasaki, K. Sakamoto, Q. Chen and S. N. Che, *Chem. Mater.*, 2006, **18**, 3904.
24 S. A. El-Safty and T. Hanaoka, *Chem. Mater.*, 2003, **15**, 2892.
25 S. Bordiga, R. Buzzoni, F. Geobaldo, C. Lamberti, E. Giamello, A. Zecchina, G. Leofanti, G. Petrini, G. Tozzola and G. Vlaic, *J. Catal.*, 1996, **158**, 486.
26 Y. M. Wang, Z. Y. Wu, H. J. Wang and J. H. Zhu, *Adv. Funct. Mater.*, 2006, **16**, 2374.
27 A. Tuel, I. Arcon and J. M. M. Millet, *J. Chem. Soc., Faraday Trans.*, 1998, **94**, 3501.
28 Y. Han, X. J. Meng, H. B. Guan, Y. Yu, L. Zhao, X. Z. Xu, X. Y. Yang, S. Wu, N. Li and F. S. Xiao, *Microporous Mesoporous Mater.*, 2003, **57**, 191.
29 Y. Li, Z. C. Feng, Y. X. Lian, K. Q. Sun, L. Zhang, G. Q. Jia, Q. H. Yang and C. Li, *Microporous Mesoporous Mater.*, 2005, **84**, 41.
30 W. Tanglumlert, T. Imae, T. J. White and S. Wongkasemjit, *Mater. Lett.*, 2008, **62**, 4545.
31 Y. C. Du, S. Liu, Y. Y. Ji, Y. L. Zhang, F. J. Liu, Q. n. Gao and F. S. Xiao, *Catal. Today*, 2008, **131**, 70.
32 Y. Wang, Q. H. Zhang, T. Shishido and K. Takehira, *J. Catal.*, 2002, **209**, 186.
33 A. Vinu, D. P. Sawant, K. Ariga, K. Z. Hossain, S. B. Halligudi, M. Hartmann and M. Nomura, *Chem. Mater.*, 2005, **17**, 5339.
34 F. Arena, G. Gatti, L. Stievano, G. Martra, S. Coluccia, F. Frusteri, L. Spadaro and A. Parmaliana, *Catal. Today*, 2006, **117**, 75.
35 M. P. Mokhonoana and N. J. Coville, *Materials*, 2009, **2**, 2337.
36 P. K. trowski, L. Chmielarz, J. Surman, E. Bidzinska, R. Dziembaj, P. Cool and E. F. Vansant, *J. Phys. Chem. A*, 2005, **109**, 9808.
37 L. Gao, F. N. Gu, Y. Zhou, J. Yang, Y. Wang and J. H. Zhu, *J. Hazard. Mater.*, 2009, **171**, 378.
38 J. H. Zhu, S. L. Zhou, Y. Xu, Y. Cao and Y. L. Wei, *Chem. Lett.*, 2003, **32**, 338.
39 Y. Xu, Z. Y. Yun, J. H. Zhu, J. H. Xu, H. D. Liu, Y. L. Wei and K. J. Hui, *Chem. Commun.*, 2003, 1894.